Earth and Planetary Science Letters 367 (2013) 39–51

Contents lists available at SciVerse ScienceDirect

Earth and Planetary Science Letters

journal homepage: www.elsevier.com/locate/epsl

The Iceland–Jan Mayen plume system and its impact on mantle dynamics in the North Atlantic region: Evidence from full-waveform inversion

Florian Rickers *, Andreas Fichtner, Jeannot Trampert

Department of Earth Sciences, Utrecht University, Budapestlaan 4, 3584 CD, Utrecht, The Netherlands

ARTICLE INFO

Article history:
Received 22 October 2012
Received in revised form
25 January 2013
Accepted 16 February 2013
Editor: Y. Ricard
Available online 15 March 2013

Keywords:
seismology
full-waveform inversion
North Atlantic
mantle plumes
Iceland
Jan Mayen

ABSTRACT

We present a high-resolution S-velocity model of the North Atlantic region, revealing structural features in unprecedented detail down to a depth of 1300 km. The model is derived using full-waveform tomography. More specifically, we minimise the instantaneous phase misfit between synthetic and observed body- as well as surface-waveforms iteratively in a full three-dimensional, adjoint inversion. Highlights of the model in the upper mantle include a well-resolved Mid-Atlantic Ridge and two distinguishable strong low-velocity regions beneath Iceland and beneath the Kolbeinsey Ridge west of Jan Mayen. A sub-lithospheric low-velocity layer is imaged beneath much of the oceanic lithosphere, consistent with the long-wavelength bathymetric high of the North Atlantic. The low-velocity layer extends locally beneath the continental lithosphere of the southern Scandinavian Mountains, the Danish Basin, part of the British Isles and eastern Greenland. All these regions experienced post-rift uplift in Neogene times, for which the underlying mechanism is not well understood. The spatial correlation between the low-velocity layer and uplifted regions suggests dynamic support by low-density asthenosphere originating from the Iceland and Jan Mayen hotspots. Our model further suggests a lower-mantle source for the Iceland and Jan Mayen hotspots. Two distinguishable low-velocity conduits are imaged, connecting the upper-mantle anomalies beneath Iceland and Jan Mayen into the lower mantle. Both conduits are tilted to the South-East, reflecting the westward motion of the Mid-Atlantic Ridge. The location of the imaged Iceland conduit is in agreement with the observation of a locally thinned transition zone south of Iceland from receiver function studies.

1. Introduction

The North American and Eurasian continental margins are drifting apart since the onset of ocean spreading in the North Atlantic about 55 Ma ago. The continental breakup went along with the eruption of large amounts of magma within a short geological time (White and McKenzie, 1989). Following the breakup, the magma production rate along the Mid-Atlantic Ridge remained locally unusually high. This resulted in the formation of Iceland (Fig. 1), which is part of an extensive bathymetric and gravimetric high observed over much of the North Atlantic (Jones et al., 2002). To the South-West of Iceland, the elevation decreases gradually along the Reykjanes Ridge towards the Charlie-Gibbs Fracture Zone. In contrast, the Kolbeinsey Ridge to the North of Iceland remains at a relatively constant, high elevation until it encounters the Jan Mayen Fracture Zone. The Jan Mayen Islands are another centre of increased magma production, possibly related to a separate hotspot. However, existing global and regional seismic models cannot resolve individual hotspots in this region (e.g. Ritsema et al., 1999; Ritsema and Allen, 2003; Bijwaard and Spakman, 1999; Grand, 2002; Pilidou et al., 2005; Legendre et al., 2012).

Considerable (kilometre-scale) post-rift uplift in Neogene times (Fig. 1) is documented on the continental shelves surrounding the North Atlantic (see summaries in e.g. Japsen and Chalmers, 2000; Doré et al., 2002; Carminati et al., 2009). Uplifted regions include, among others, the southern and northern Scandinavian Mountains in western Scandinavia (Rohrman et al., 1995; Redfield et al., 2005), part of the British Isles (George, 1966; Green, 1989; Japsen, 1997; Duncan et al., 1998; Hall and Bishop, 2002; Holford et al., 2008), the Danish Basin (Japsen et al., 2002, 2007), eastern Greenland (Mathiesen et al., 2000; Johnson and Gallagher, 2000) and Svalbard (Vågnes and Amundsen, 1993). Deep cratonic roots, which could isostatically balance the additional topography, are lacking beneath these regions. The mechanism for the uplift is debated (e.g. Rohrman and van der Beek, 1996; Ebbing and Olesen, 2005; Holford et al., 2008; Pascal and Olesen, 2009; Ebbing et al., 2012). A connection to the Iceland hotspot is supported by the tomographic study of Weidle and Maupin (2008), who image

* Corresponding author. Tel.: +49 173 8321531.
E-mail addresses: florian.rickers@gmail.com (F. Rickers), A.Fichtner@uu.nl (A. Fichtner), J.A.Trampert@uu.nl (J. Trampert).

0012-821X © 2013 Elsevier B.V. Open access under CC BY-NC-ND license.
http://dx.doi.org/10.1016/j.epsl.2013.02.022

a low-velocity finger extending beneath the lithosphere to the southern Scandinavian Mountains. Beneath parts of the British Isles, Arrowsmith et al. (2005) image low velocities, and Davis et al. (2012) find a negative correlation between crustal thickness and topography. Both of these studies indicate dynamic support, which they suggest to be related to low-density material from the Iceland hotspot. Scaled long-wavelength gravity maps (Jones et al., 2002) indicate that parts of Britain, southern Scandinavia and eastern Greenland are presently experiencing dynamic support related to the Iceland hotspot.

Morgan (1971) proposed that the localised, long-lived magmatism of hotspots could be caused by mantle plumes. They are envisioned as narrow, hot upwellings originating from the core-mantle boundary. In the case of Iceland, a possible mantle plume would be interacting with a spreading ridge, and might have weakened the continental lithosphere prior to continental breakup. The mantle plume hypothesis found widespread acceptance, but unambiguous seismic evidence for the continuation of upper-mantle low-velocity anomalies into the lower mantle beneath Iceland is still sparse.

Some global tomographic models show broad and relatively weak low-velocity structures in the lower mantle below Iceland (e.g. Bijwaard and Spakman, 1999; Ritsema et al., 1999; Zhao, 2004), which cannot be interpreted with certainty as continuous plume structures. Several studies attempted to image the mantle below Iceland using array data recorded on Iceland (Tryggvason et al., 1983; Wolfe et al., 1997; Foulger et al., 2001; Allen et al., 2002; Bjarnason et al., 2002; Delorey et al., 2007). While all these models agree on the presence of low velocities in the uppermost mantle, results are contradictory in deeper mantle regions. Keller et al. (2000) showed that the limited array aperture used in such studies does not permit unique constraints on the depth extent of the Iceland anomaly. Using receiver functions, Shen et al. (1998, 2002) imaged a locally thinned transition zone below Iceland, indicative for elevated temperatures which could possibly be caused by a hot plume. Other studies, however, imaged a flat transition zone using similar methods (Du et al., 2006).

Hwang et al. (2011) find that simple cross-correlation travel-time measurements are not suited to extract lower-mantle plume information from seismic data. Rickers et al. (2012) come to the same conclusion and explain it with the fact that such methods do not account for diffraction effects in seismic wave propagation, which are strong in the case of small-scale heterogeneities.

The lack of unambiguous evidence for a lower-mantle plume below Iceland leaves the possibility of a different mechanism producing the increased magma volumes. Such a mechanism could be fertile, old crust in the upper mantle, being overridden by the Mid-Atlantic Ridge (Foulger et al., 2001; Foulger and Anderson, 2005; Foulger, 2012).

The need for an improved tomographic model of the whole North Atlantic region, covering the upper and at least part of the lower

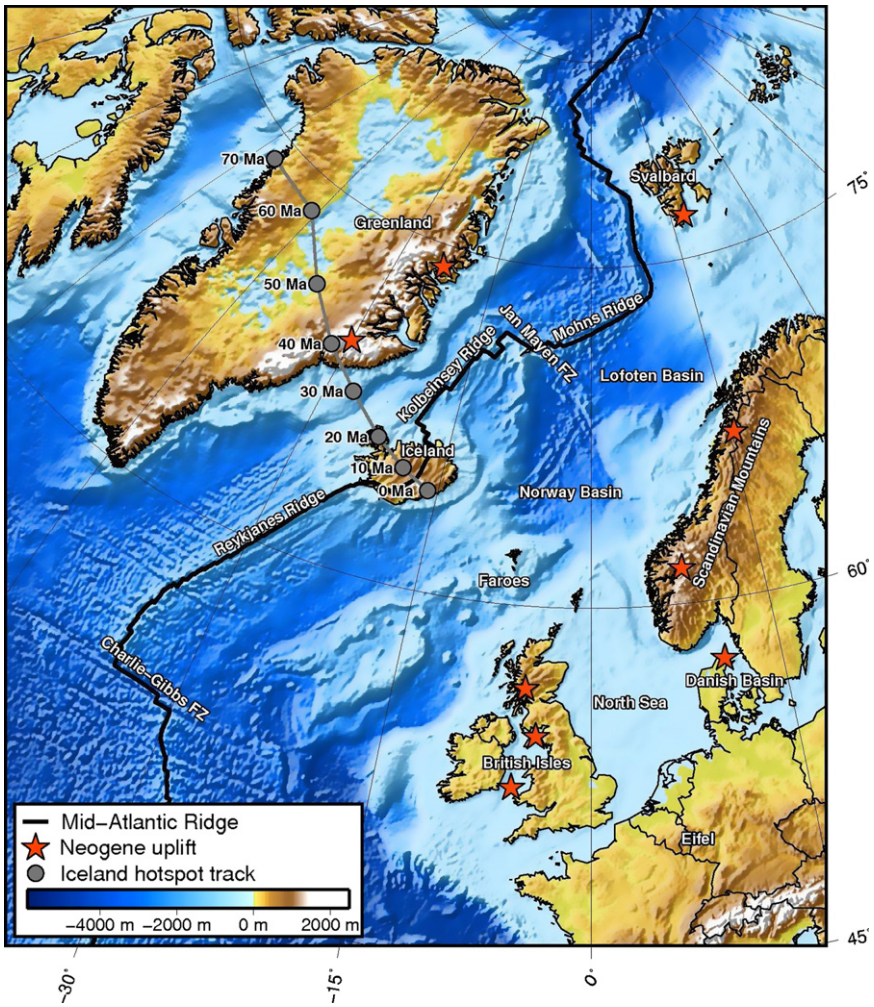

Fig. 1. Bathymetry and topography of the North Atlantic region. The black line indicates the Mid-Alantic Ridge, the grey dots represent the reconstructed Iceland hotspot track between 70 Ma and today (Lawver and Müller, 1994). Red stars indicate a (non-complete) selection of regions where Neogene uplift is documented (after Japsen and Chalmers, 2000; Japsen et al., 2007; Holford et al., 2008, and references therein). FZ is used as abbreviation for Fracture Zone. (For interpretation of the references to colour in this figure caption, the reader is referred to the web version of this article.)

mantle, motivated this study. Our model is based on non-linear full-waveform inversion techniques and measurements of the instantaneous phase misfit. This method has been shown to overcome limitations of classical linearised tomography and to potentially improve tomographic resolution in both the upper as well as the lower mantle (Fichtner and Trampert, 2011; Rickers et al., 2012).

2. Method, data and inversion

2.1. Tomographic method

The inversion is based on a non-linear iterative conjugate gradient optimisation scheme (Fletcher and Reeves, 1964). Gradients are computed with the adjoint method (Tarantola, 1984; Tromp et al., 2005; Fichtner et al., 2006), and the misfit between synthetic and observed seismograms is quantified by their instantaneous phase difference (Bozdağ et al., 2011; Rickers et al., 2012). This misfit is a time-dependent and amplitude-independent measurement of waveform differences. In contrast to traditional tomographic methods, it allows for the consideration of smaller-amplitude phases such as diffracted waves in an inversion. The proper treatment of diffracted waves improves resolution and is essential for the imaging of small-scale anomalies such as plumes, in particular in the lower mantle (Rickers et al., 2012). The aim of the inversion is the iterative minimisation of a misfit function χ, which for a current model m is defined as

$$\chi(m) = \frac{1}{2}\sum_{i=1}^{N}\int_0^T \|\phi_i^{synt}(t,m) - \phi_i^{obs}(t)\|^2\, dt, \quad (1)$$

where $\phi_i^{synt}(t,m)$ and $\phi_i^{obs}(t)$ denote the instantaneous phase of the (windowed) synthetic and observed seismogram i at time t, respectively. The total number of seismograms used in the inversion is N, the end time of the synthetic seismograms is T. For a detailed derivation of the instantaneous phase misfit, the reader is referred to Bozdağ et al. (2011).

The forward and adjoint synthetic wavefields are computed with the spectral element code SES3D (Fichtner and Igel, 2008), which accurately solves the elastic wave equation in strongly heterogeneous, three-dimensional media. Similar techniques have been successfully applied in recent regional full-waveform tomographic studies (e.g. Fichtner et al., 2009; Tape et al., 2010; Zhu et al., 2012). This study is the first real data application of the instantaneous phase misfit, which has been demonstrated to potentially resolve lower-mantle plumes in preceding synthetic studies (Rickers et al., 2012).

2.2. Model setup

The model covers all of Europe, Greenland, as well as parts of Canada and Russia, spanning a distance of 6000 × 6000 km in the lateral directions. The covered area is marked by the black outline in Fig. 2(a). In the vertical direction, the model extends down to a depth of 1300 km. While the actual region of interest is smaller and restricted to the North Atlantic and the adjacent regions, the large model area improves azimuthal ray coverage because events occurring in southern Europe can be included in the inversion, in addition to the events at the Mid-Atlantic Ridge. Furthermore, larger epicentral distances improve the illumination of the lower mantle by body waves.

The model is divided into blocks with a horizontal spacing of 100 km and a depth-dependent vertical spacing of 10 km in the uppermost 350 km, 20 km between 350 km and 700 km depth and 50 km between 700 and 1300 km depth. This honours the steeper vertical velocity gradients and the higher resolution in the uppermost mantle.

We invert for both the horizontally and vertically polarised S-wave velocity β_{sh} and β_{sv}, which is necessary to fit Rayleigh- as well as Love-waves. The P-wave velocity α, the density ρ and the attenuation Q are kept at the initial values of the starting model throughout the inversion. We base the discussion of the model on the β_{sh}-component of the S-velocity, which our resolution tests indicate to be better resolved.

2.3. Starting model and 1-D reference model

Phase measurements, such as the instantaneous phase difference used in this study to quantify waveform misfits, require synthetic and observed waveforms to be within half a period of each other. An accurate starting model is therefore important. It increases the number and length of measurement windows that meet this requirement at the beginning of the inversion and accelerates the convergence towards the optimum model. We used the European full-waveform model developed by Fichtner and Trampert (2011) as starting model. It is based on time-frequency misfits of surface- and body-waves with a minimum period of 60 s. In the remainder of this paper, we refer to it as EU-TF (Europe-Time Frequency). Coherently, we refer to our final model as NA-IP (North Atlantic-Instantaneous Phase). Model

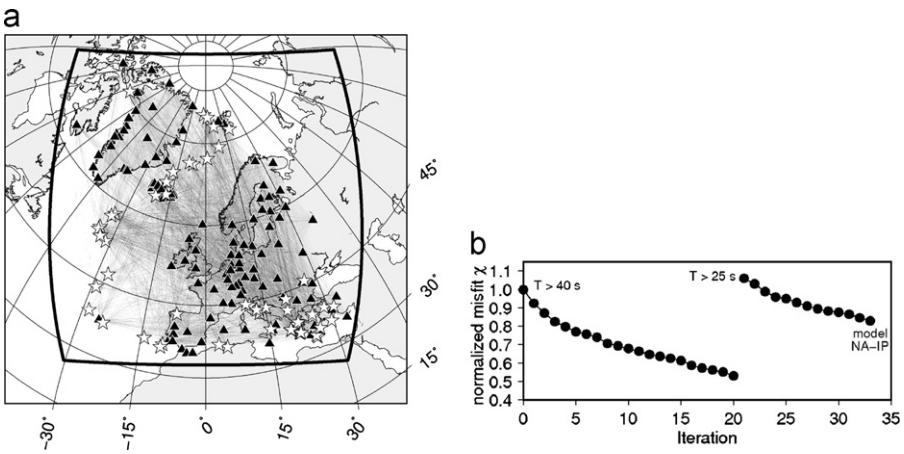

Fig. 2. (a) Events (white stars) and receivers (black triangles) used for the inversion. The thin lines represent the great-circle ray paths of the data. The black outline indicates the model boundaries. (b) Normalised value of the misfit function χ as a function of the number of iterations. The normalisation, for the purpose of clarity of the plot, is with respect to the initial value of χ at iteration 0. Up to iteration 20, the minimum period of the seismograms is 40 s. From iteration 21, the minimum period is 25 s.

slices presented throughout this paper show velocity perturbations with respect to a 1-D reference model. This reference model is a modified version of PREM (Dziewonski and Anderson, 1981), with a linear gradient replacing the 220 km discontinuity (Fichtner and Trampert, 2011).

2.4. Data

We used a carefully chosen set of high-quality seismic waveform data covering the North Atlantic region, including a substantial amount of body waves sampling the lower mantle. We selected 60 events with magnitudes above Mw 5.4, aiming at a good azimuthal coverage. Data were obtained from the *Incorporated Research Institutions for Seismology* (*IRIS*) and the *Observatories and Research Facilities for European Seismology* (*ORFEUS*). Station networks include the *Greenland Ice Sheet Monitoring Network* (*GLISN*), the *Greenland Lithosphere Analysed Teleseismically on the Ice Sheet* (*GLATIS*) *Network* and the *Iceland HOTSPOT Network*, which together with stations in continental Europe provided a good coverage of the whole North Atlantic region. The distribution of events and receivers and the ray coverage are shown in Fig. 2(a).

Because of the natural distribution of earthquakes and the uneven coverage of the region with seismic stations, a bias in the ray coverage cannot be avoided. The iterative inversion scheme can balance a possible bias to a certain degree, but this comes at the cost of a slower convergence of the misfit function. Careful initial weighting of the data can therefore accelerate the inversion. We attempted to correct for the uneven data coverage by manually adjusting the relative weight of stations in the inversion. Based on a visual inspection of the ray coverage and the local station density, the weight of the individual stations was adjusted within a range of $\pm 50\%$ with respect to their initial weight.

2.5. Inversion

Prior to the start of the inversion, we filtered the observed and synthetic seismograms in a period range between 40 and 200 s. All three components were used, and we selected 4366 high-quality seismograms which allowed for meaningful measurements. We manually selected measurement windows where data and synthetics are within half a period of each other, and computed the instantaneous phase difference and corresponding adjoint sources (Tromp et al., 2005; Bozdağ et al., 2011; Rickers et al., 2012). The convergence of the misfit function χ as a function of the number of iterations is shown in Fig. 2(b). After 20 iterations, the initial misfit had decreased by almost 50%. At this stage of the inversion, we increased the frequency content of the seismograms to a minimum period of 25 s. We again selected measurement windows and performed 13 more iterations. While the misfit initially increased at iteration 21 due to the higher frequency content and changed measurement windows, it had decreased again by about 25% at the final iteration.

3. Validation

The inversion scheme is non-linear, which on the one hand allows for the inclusion of complex wave propagation effects leading to better-constrained models. On the other hand, it is difficult to assess the resolution of the resulting model because there is no simple operator relating inversion input and model output. We estimate the validity of the model in different ways. These are (1) a visual inspection of the global S-velocity model S20RTS (Ritsema et al., 1999), the initial model EU-TF (Fichtner and Trampert, 2011) and the presented model NA-IP, (2) a comparison of waveform fits for these three models, and (3) a linearised resolution analysis for specific regions of the model using Point Spread Functions (Fichtner and Trampert, 2011).

3.1. Visual inspection

A visual inspection of horizontal model slices at a depth of 80 km is presented in Fig. 3. We show the global mantle model S20RTS (Ritsema et al., 1999) along with the full-waveform models because S20RTS served as starting model to construct EU-TF (Fichtner and Trampert, 2011), which was then used as starting model to derive NA-IP. It is apparent that the imaged details increase from the smooth global model S20RTS via the European full-waveform model EU-TF to the final North Atlantic model NA-IP. While in S20RTS, a smooth low-velocity zone covers the region around Iceland, in EU-TF it narrows down on Iceland and Jan Mayen and the two hotspots become distinguishable. Other features along the Mid-Atlantic Ridge are not well-defined, however. The higher frequency content, incorporation of

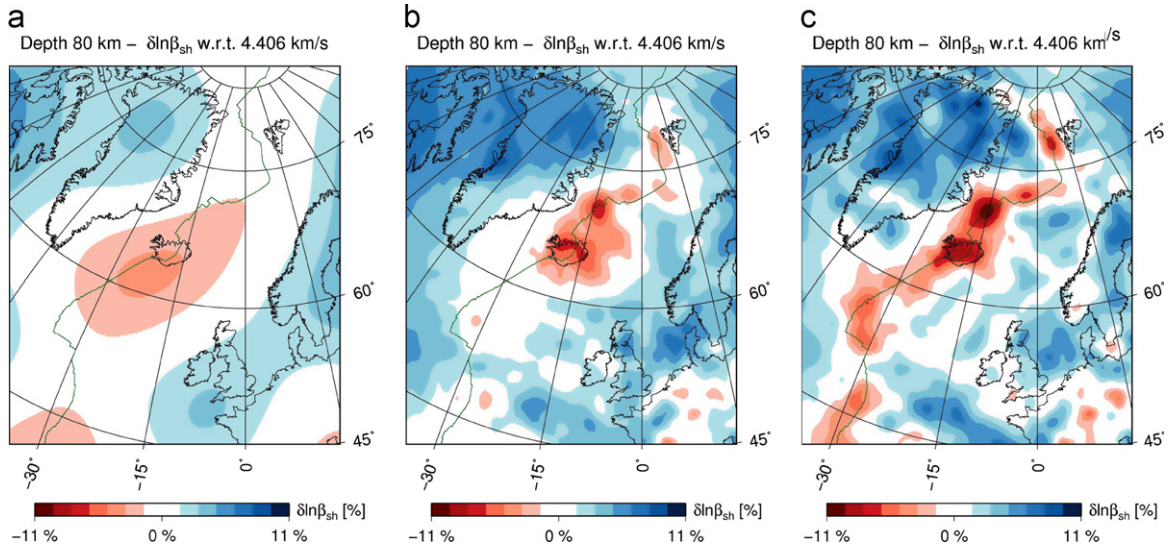

Fig. 3. Horizontal slices through three different models at 80 km depth beneath the North Atlantic region. (a) Global S-velocity model S20RTS (Ritsema et al., 1999), (b) β_{sh}-component of full-waveform starting model EU-TF (Fichtner and Trampert, 2011) (which itself was constructed using S20RTS as starting model) and (c) β_{sh}-component of presented model NA-IP.

regional data and possibly the choice of misfit in the present study eventually lead to a well-defined Mid-Atlantic Ridge in the final model NA-IP. High-velocity features, such as the Greenland and Baltic Shields as well as the North Sea, also become more pronounced. The correlation of imaged velocity perturbations with topographic and tectonic features (Fig. 1) indicates the geologic plausibility of the model, at least in the upper part.

An interesting observation is the much stronger perturbation amplitude of models derived with non-linear full-waveform methods (compare S20RTS and NA-IP in Fig. 3). While differences in regularisation and parameterisation certainly contribute to the difference in amplitude between the models, the occurrence of higher amplitudes in full-waveform models is also a result of the consideration of diffraction effects. While in classical linearised inversions, these effects are not properly accounted for and consequently do not contribute significantly to the model, diffracted waves are focused back onto their source region in non-linear full-waveform inversions, leading to a much better recovery of the perturbation amplitude (see Rickers et al., 2012). A higher frequency content enhances this effect for small-scale structures, explaining the difference in perturbation strength of, for instance, the Iceland hotspot between models EU-TF and NA-IP.

3.2. Waveform fits

Improved waveform fits are another indicator of an improved model. In Fig. 4, examples are presented for a Mw 6.0 event which occurred in Turkey on September 19, 2011. This event is one of the events that was used in the inversion. Synthetic waveforms computed in models S20RTS, EU-TF and NA-IP are compared to the corresponding data recorded at different stations. The waveforms are filtered at periods between 25 and 200 s and contain S-waves and surface-waves as well as their reflections and diffractions. The improved waveform fit of the presented model NA-IP is evident, and in many cases every wiggle within the measurement window could be closely fitted to the data. We note that the amplitude fit improves along with the phase, even though we did not explicitly invert the amplitude information.

3.3. Point Spread Functions

A more quantitative method to assess the resolution of tomographic models derived with non-linear inversion techniques are Point Spread Functions (PSFs) (Fichtner and Trampert, 2011). A PSF indicates how well a small, localised structure in the final model is resolved, and in particular it reveals if trade-offs with structure elsewhere in the model exist. The panels in Fig. 5(a) show two

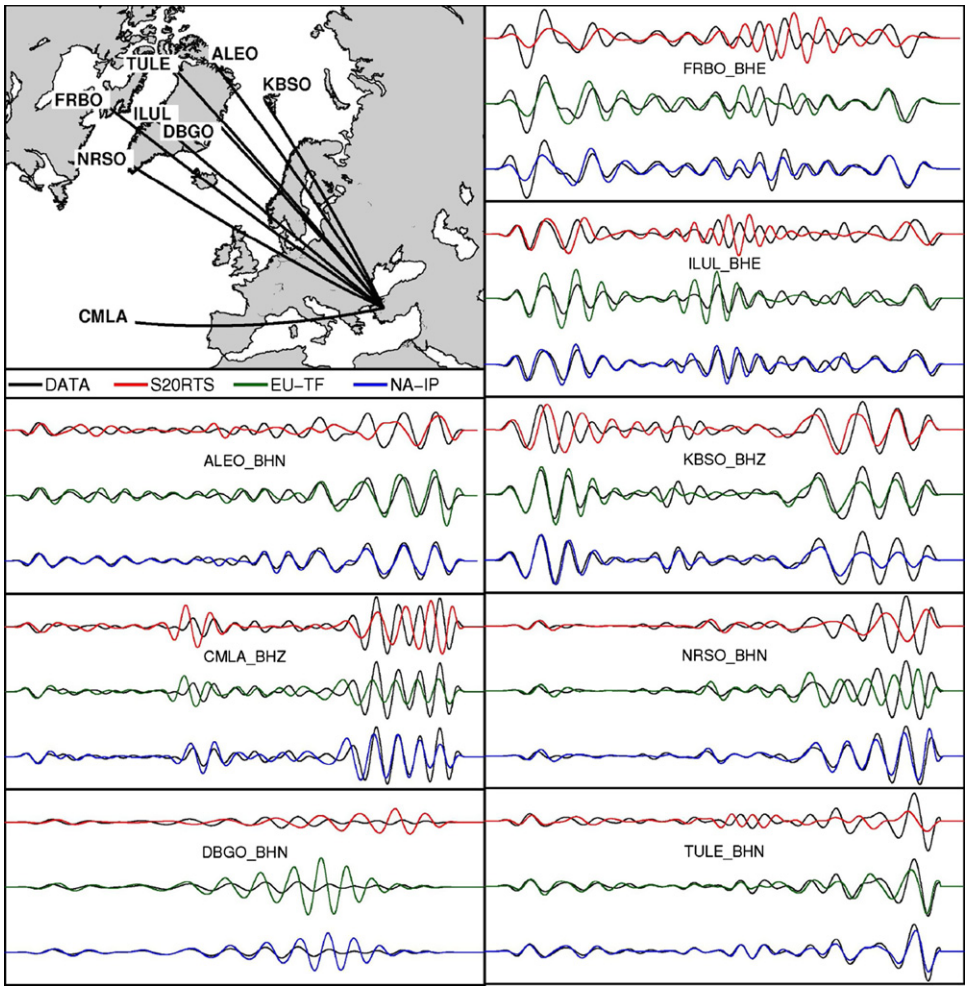

Fig. 4. Waveform fit between synthetics and data for different models. Synthetics are computed in the global model S20RTS (Ritsema et al., 1999) (red), in the full-waveform starting model EU-TF (Fichtner and Trampert, 2011) (green) and in the presented model NA-IP (blue). The data (black) are from a Mw 6.0 event in Turkey on September 19, 2011, recorded at different stations. The presented waveforms are S- and surface-waves, including their reflections and diffractions, at a minimum period of 25 s. (For interpretation of the references to colour in this figure caption, the reader is referred to the web version of this article.)

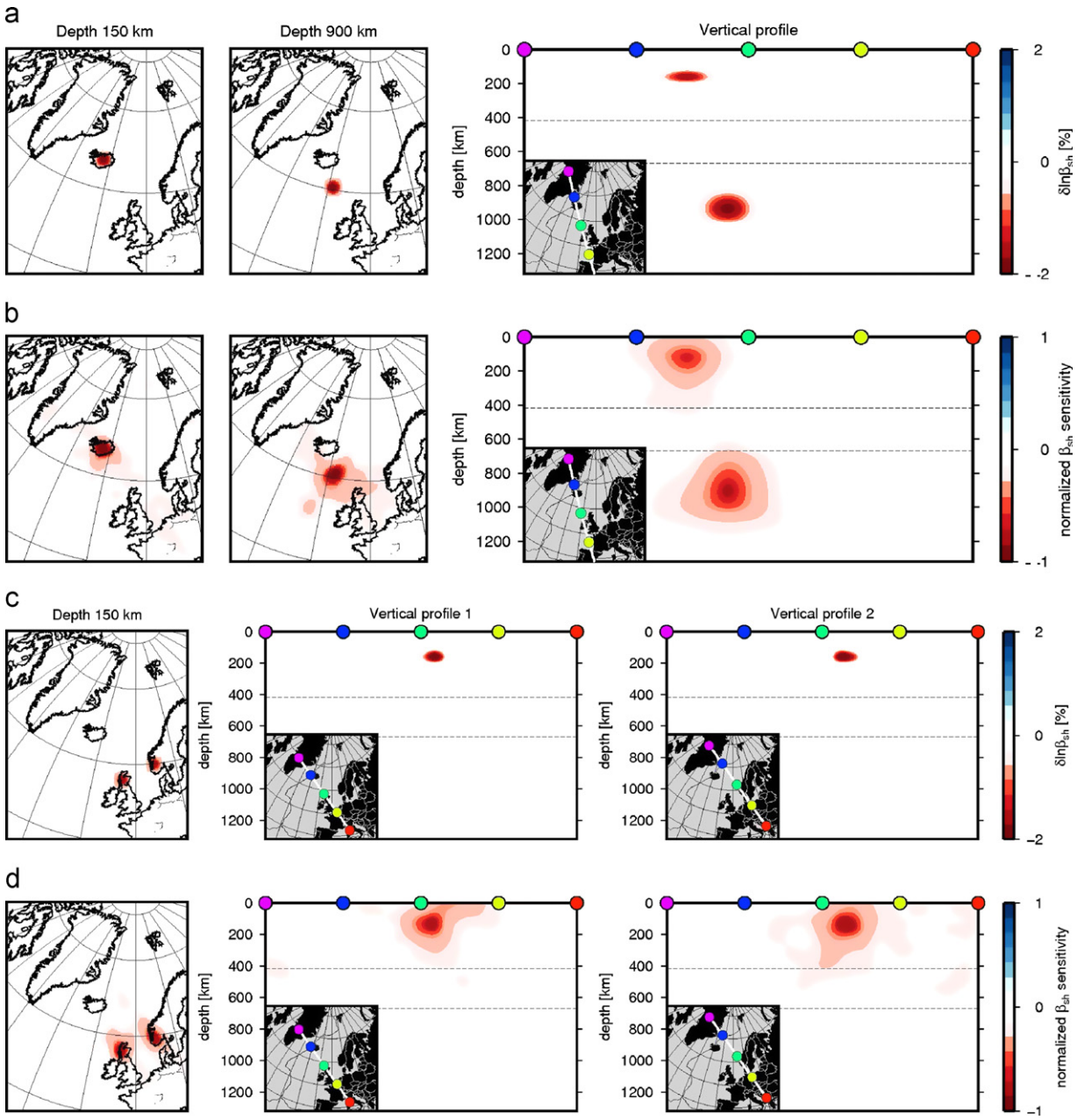

Fig. 5. Two examples for local resolution tests with Point Spread Functions (PSFs). (a) Test 1—input: two smoothed point perturbations of the SH-velocity β_{sh} at depths of 150 km and 900 km below Iceland. The perturbations are superimposed onto the final model NA-IP. The two panels on the left show horizontal slices through the perturbations at depths of 150 km and 900 km, the panel on the right shows a vertical slice through both perturbations. (b) Test 1—output: PSFs showing the sensitivity of the β_{sh}-component as a response to the perturbations. (c) Test 2—input: two smoothed point perturbations in β_{sh} at a depth of 150 km. The panel on the left shows a horizontal slice through the perturbations at a depth of 150 km, the two panels on the right show vertical slices through each of the perturbations. (d) Test 2—output: PSFs showing the sensitivity of the β_{sh}-component as a response to the perturbations.

smoothed, localised perturbations in β_{sh}, which is the velocity of horizontally polarised S-waves. The diameter of the perturbations is $\sim$200 km, and they are centred at depths of 150 km and 900 km below Iceland. The perturbations are superimposed onto the final model NA-IP. The chosen location of the perturbations corresponds to locations where low velocities are imaged in model NA-IP. A confirmation that these structures are well-resolved and no strong trade-offs exist could justify an interpretation in terms of an Iceland plume. Trade-offs in the form of smearing can lead to apparent plume-like structure in tomographic images beneath hotspot regions (Keller et al., 2000). The panels in Fig. 5(b) show the resulting PSFs for the β_{sh}-component. The two perturbations are clearly distinguishable and the location of their maximum amplitude has not changed, indicating that imaged structures at these locations are well-resolved. In the two bottom panels of Fig. 5, we present a second test at two different locations at a depth of 150 km, corresponding to two prominent low-velocity structures in model NA-IP (see Section 4.3). The diameter of the smoothed point perturbations in β_{sh} is $\sim$150 km (Fig. 5(c)). The resulting PSFs in Fig. 5(d) again indicate that the model is well-resolved at the tested locations. We calculated PSFs for a number of different locations and depths, consistently indicating that the β_{sh}-component of our model is well-resolved. In contrast, we find that the β_{sv}-component is less well-resolved in the deeper part of the model.

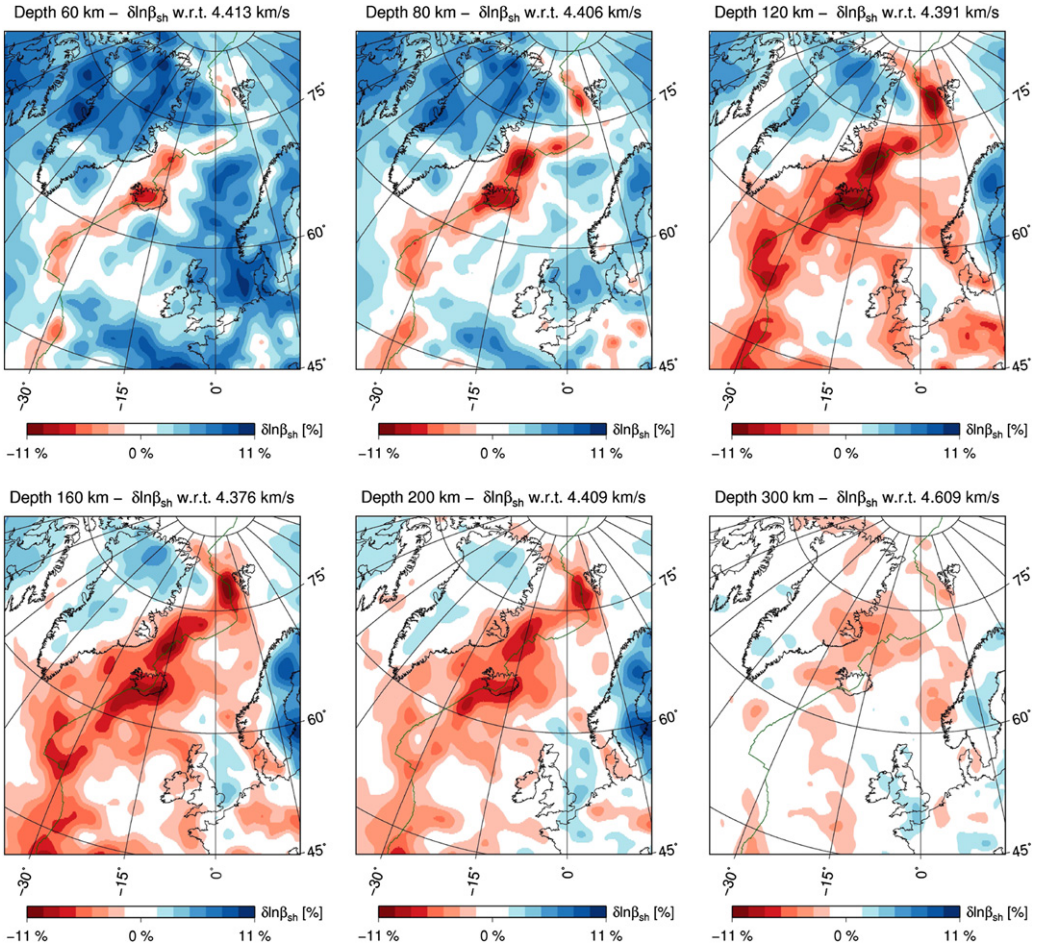

Fig. 6. Horizontal slices through the β_{sh}-component of model NA-IP, at depths between 60 and 300 km. Perturbations are with respect to the reference velocity indicated in each panel.

4. Model

In this section, the β_{sh}-component of model NA-IP is presented. The discussion is divided into four parts, each focusing on a particular feature of the model. These are (1) the cratons and ocean basins, (2) the Mid-Atlantic Ridge and the Iceland and Jan Mayen hotspots, (3) a sub-lithospheric low-velocity layer beneath oceanic and continental lithosphere, and (4) low-velocity conduits beneath the Iceland and Jan Mayen hotspots, suggesting a lower-mantle source.

4.1. Cratons and ocean basins

In Fig. 6, horizontal slices of the model at depths between 60 and 300 km are presented. Prominent high-velocity features are the thick cratonic Greenland and Baltic Shields. They are imaged in numerous studies (e.g. Pilidou et al., 2005; Ritsema et al., 2011; Legendre et al., 2012), and are recovered sharply and with great detail in our model. The cratonic roots are deepest in northern and south-western Greenland, where they extend to about 160–200 km depth. Towards eastern Greenland, their thickness decreases to below 100 km, which is better visible from the western part of the vertical slices in Fig. 7. An East–West oriented corridor of reduced lithospheric thickness is imaged across Greenland, which is particularly apparent at depths between 120 and 200 km (Fig. 6). Its location approximately correlates with the reconstructed track of the Iceland hotspot between 70 and 40 Ma ago (see Fig. 1) (Morgan, 1983; Lawver and Müller, 1994), which may have caused weakening and thinning of the lithosphere along its track.

The Baltic Shield is characterised by high velocities to depths of more than 200 km. Our model shows a sharp boundary between the deep Precambrian lithosphere of the Baltic Shield and the much shallower lithosphere of South-West Norway and the Danish Basin. This is particularly apparent from the eastern end of the vertical slice in Fig. 7(b), which cuts into the Baltic Shield of southern Sweden. High velocities are further imaged beneath the North Sea and, to a lesser extent, beneath the Lofoten and Norway Basins.

4.2. The Mid-Atlantic Ridge and the Iceland and Jan Mayen hotspots

At shallow depths between 60 and 80 km (Fig. 6), low velocities are imaged within a narrow band to both sides of the Mid-Atlantic Ridge, where new ocean floor is being created and the oceanic lithosphere is thinnest. Two regions of anomalously low velocities are centred beneath Iceland and beneath the northern Kolbeinsey Ridge, just south of the Jan Mayen Fracture Zone. Velocities here are reduced by up to −11% with respect to the 1-D reference model. At depths between 100 and 200 km, these two low-velocity regions are still clearly distinguishable. At these depths, the Iceland anomaly is elongated in the direction of the Reyjkanes Ridge, with a slight tilt to the South. The Jan Mayen anomaly covers the whole length of the Kolbeinsey Ridge and extends beyond the Jan Mayen Fracture Zone to the southern Mohns Ridge. Velocity perturbations in those along-ridge regions

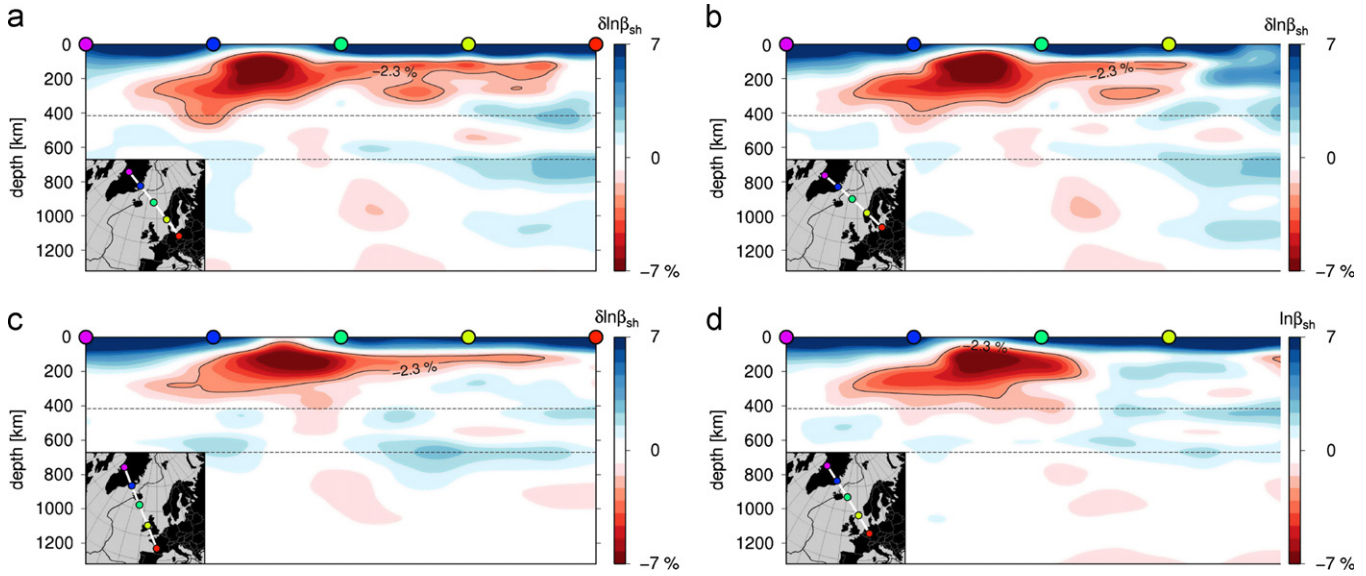

Fig. 7. Vertical slices through the β_{sh}-component of model NA-IP. The slices are roughly perpendicular to the Mid-Atlantic Ridge, the exact location is shown in the overview map in each panel. The black contours indicate perturbations of −2.3% with respect to the 1-D reference model. Slices (a) and (c) cut roughly along the sub-lithospheric low-velocity fingers extending into Scandinavia and the British Isles, respectively. Slice (b) cuts slightly north of the Scandinavian low-velocity finger and into to the Baltic shield. Slice (d) cuts inbetween the two low-velocity fingers through the (high-velocity) North Sea.

reach between −7% and −11%. Below a depth of ∼250 km, perturbations are much weaker and no longer centred beneath the ridge.

The elevated magmatism in the region of the Jan Mayen Islands and the unusually high elevation of the Kolbeinsey Ridge along its whole length indicate the presence of a separate hotspot. This is supported by geochemical isotope studies (Schilling, 1985; Schilling et al., 1999), which suggest different sources of the basalts in the regions of Iceland and Jan Mayen. They propose that the boundary between the influence zones of the Iceland and the Jan Mayen hotspots is located about halfway along the Kolbeinsey Ridge between Iceland and Jan Mayen.

Most existing global and regional tomographic models image low velocities in the Iceland - Jan Mayen region (e.g. Bijwaard and Spakman, 1999; Ritsema et al., 2011; Pilidou et al., 2005; Legendre et al., 2012). The regional surface-wave model of Pilidou et al. (2005) appears to have the best resolution among these models. They image an elongated low-velocity zone centred on Iceland, extending ∼1700 km along-ridge and ∼600 km across at 100 km depth. However, the resolution of their model is not sufficient to constrain the anomaly further, and to make a statement regarding a possible separation of the Iceland and Jan Mayen hotspots.

Resolution tests using PSFs indicate that both hotspots are well-resolved. Our model favours the boundary between the hotspots to be located just to the North of Iceland.

To the South-West of Iceland, the deviation of the low-velocity anomaly with respect to the Reykjanes ridge may be related to radial anisotropy and the fact that the presented model is a β_{sh}-model. Delorey et al. (2007) find an anomalously strongv (∼5%) and asymmetric (stronger on the European than on the North American side) $\beta_{sv} > \beta_{sh}$—anisotropy pattern in the upper 100 km beneath the Reykjanes Ridge, peaking at a distance of ∼120 km parallel to the ridge axis on the European side. Their model represents an along-axis average over the length of the Reykjanes ridge and does not constrain along-ridge variations such as the increasing tilt away from Iceland that is imaged in our model. The resolution of their anisotropy model however does not extend below ∼100 km depth, where the observed pattern is strongest in our model.

4.3. Sub-lithospheric low-velocity layer beneath oceanic and continental lithosphere—connection to Neogene uplift?

Velocity perturbations are strongest in the vicinity of the hotspots along the Mid-Atlantic Ridge, but a low-velocity layer is imaged beneath much of the oceanic lithosphere of the North Atlantic. It locally extends beneath the continental lithosphere. This suggests a flow of low-velocity hotspot material not only along-ridge, but also in directions away from the Mid-Atlantic Ridge over long distances.

Particularly intriguing are two low-velocity fingers at depths between 120 and 180 km (Fig. 6), reaching from the hotspot region far into the continental lithosphere. One finger extends towards South-West Norway and further beneath the Danish Basin. The other finger stretches along the British Isles to the tip of Brittany, roughly following the line defined by the Irish Sea between Ireland and the eastern British Isles. These two low-velocity fingers are separated by the North Sea, below which weakly positive velocities are imaged.

The vertical slices in Fig. 7 yield a clearer image of these sub-lithospheric low-velocity fingers and their connection to the Iceland and Jan Mayen hotspots. The slice in Fig. 7(a) cuts through the northern Kolbeinsey Ridge and follows the Scandinavian finger to Denmark. The low-velocity material forms a layer below the lithosphere. The layer thickness, defined by a velocity reduction of more than −2.3%, is approximately 60–80 km. Locally, in particular beneath South-West Norway, the layer is considerably thicker. This may be caused by a branch of the Jan Mayen plume (see Section 4.4 for details). A slice slightly further north (Fig. 7(b)) indicates that the low-velocity layer is confined to the shallow lithosphere of South-West Scandinavia. It does not extend beneath the thicker Precambriam lithosphere of the Baltic Shield.

The vertical slice in Fig. 7(c) cuts through Iceland and along the finger beneath the British Isles. The low-velocity layer is slightly thinner and weaker than the layer below southern Scandinavia. It is not thickened locally. A vertical slice through Iceland and the North Sea (Fig. 7(d)), in-between the two fingers, shows that the low-velocity layer does not extend eastward beyond the Faroe Islands. Instead, weakly positive velocity perturbations are

imaged beneath the lithosphere of the North Sea. The low-velocity region at the eastern end of the slice is related to the Eifel volcanic zone.

It appears that lithospheric thickness does not increase notably with growing distance from the Mid-Atlantic Ridge where the sub-lithospheric low-velocity layer is present. In contrast, the slice through the North Sea shows an increase in lithospheric thickness away from the ridge. This suggests the existence of thin-lithosphere channels beneath the oceanic and continental lithosphere, along which the hot asthenosphere flows over long distances.

The presence of the sub-lithospheric low-velocity layer in our model beneath regions of major (kilometre-scale) post-rift Neogene uplift (Fig. 1) suggests dynamic support of the uplifted regions. A correlation is particularly evident for the British Isles and South-West Scandinavia.

Dynamic support of post-rift uplifted regions by hotspot-related low-density material has been proposed by various authors (e.g. Rohrman and van der Beek, 1996; Jones et al., 2002; Bott and Bott, 2004). This may explain the lack of deep crustal roots which normally isostatically balance elevated topography.

A number of smaller-scale tomographic studies confirm the presence of low velocities beneath uplifted regions. Weidle and Maupin (2008) image a sub-lithospheric low-velocity finger reaching from the region of the Iceland hotspot to southern Scandinavia. They are careful with their interpretation, however, because their model shows a continuation of the low-velocity anomaly into southern Sweden, where other models image the much thicker cratonic lithosphere of the Baltic Shield. Their imaged finger is consistent with our model, except that we do not image a continuation of the low-velocity layer beneath the Baltic Shield. Our model shows a continuation of the finger into the Danish Basin, along the southern boundary of the Baltic Shield. In the Danish Basin, Neogene uplift (and successive erosion) is documented (Japsen et al., 2002, 2007).

Beneath the northern and central British Isles, Arrowsmith et al. (2005) image a region of reduced compressional wave velocities which they attribute to a low-velocity finger from the Iceland hotspot. Davis et al. (2012) find a northward decrease in crustal thickness beneath Britain, which negatively correlates to average elevation. They argue for the presence of a low-velocity layer beneath the lithosphere, providing isostatic support of the elevated regions.

For the regions of the British Isles and Southern Scandinavia, the correlation of the sub-lithospheric low-velocity layer with Neogene uplift is most apparent. Low velocities are further imaged at depths between $\sim$100 km and 400 km beneath the cratonic lithosphere of eastern Greenland, possibly isostatically balancing the major Neogene uplift documented in this region. The Neogene uplift of the northern Scandinavian Mountains may be caused by a different mechanism than the uplift of the southern Scandinavian Mountains, unrelated to mantle processes (Ebbing and Olesen, 2005). This would be consistent with our model, which does not show a low-velocity layer beneath the northern Scandinavian Mountains. Svalbard, where major Neogene uplift is also documented, is located at the edge of the well-sampled part of our model. A strong low-velocity anomaly is imaged to its West beneath the Mid-Atlantic Ridge. The anomaly appears to extend beneath the western part of Svalbard, but the resolution at the edge of the model may not be sufficient to confidently confirm a correlation.

The pattern of the low-velocity layer imaged in our model correlates well with estimates of present-day dynamic support by Jones et al. (2002). Their estimations are based on scaled versions of the long-wavelength ($>$800 km) free-air gravity anomaly field. In Fig. 8, we show an updated figure from Jones et al. (2002) based on the more recent GRACE gravity data (Tapley et al., 2007). As described in Jones et al. (2002), the appropriate scaling factors Z are different for sub-aqueous (Fig. 8(a), $Z=35$ mGal km^{-1}) and sub-aerial (Fig. 8(b), $Z=50$ mGal km^{-1}) regions. To facilitate a comparison with our model, Fig. 8(c) shows the averaged velocity perturbation of model NA-IP in the depth range between 100 km and 200 km. This depth range covers much of the sub-lithospheric low-velocity layer at the European side of the Mid-Atlantic ridge, as well as the low velocities beneath the Mid-Atlantic ridge. It does not cover the deeper low-velocity layer beneath Greenland. Similar to the gravity field, the averaged velocity has been low-pass filtered through convolution with a Gaussian of width 800 km.

It is apparent that the estimations of present-day dynamic support correlate to the imaged sub-lithospheric low-velocity

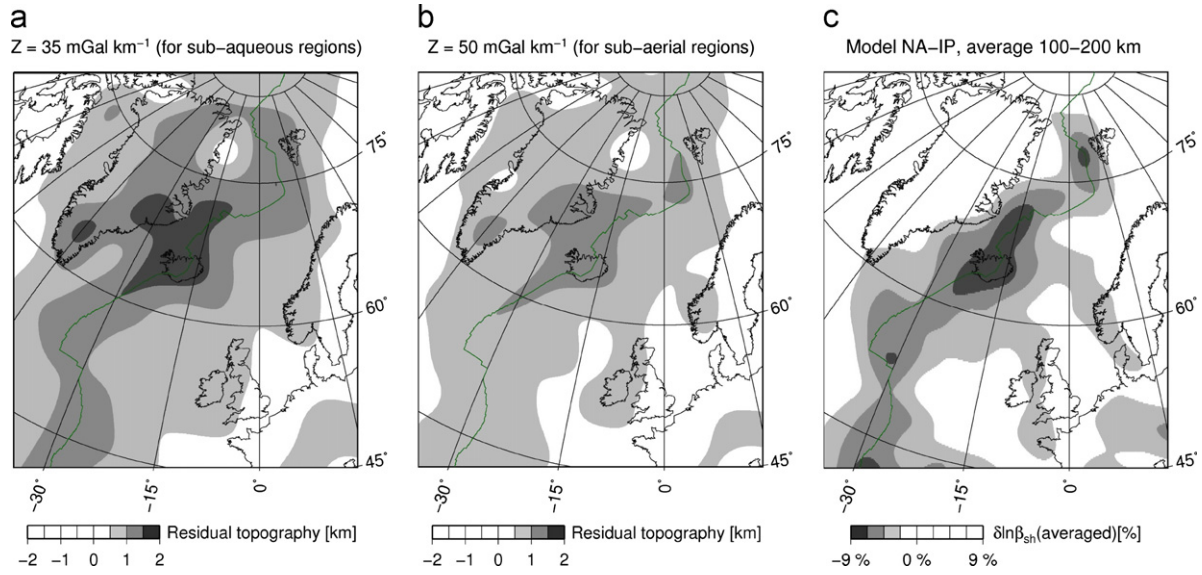

Fig. 8. (a and b) Estimates of present-day dynamic support in the North Atlantic region, calculated according to (Jones et al., 2002) through division of the long-wavelength free-air gravity anomaly field by a constant admittance Z. For estimates of dynamic support in sub-aqueous regions, $Z=35$ mGal km^{-1} is considered appropriate, for sub-aerial regions $Z=50$ mGal km^{-1}. (c) Long-wavelength average velocity perturbation between 100 km and 200 km depth of model NA-IP. To facilitate comparison with the estimated dynamic support, the average velocity is lowpass-filtered by convolution with a Gaussian of width 800 km.

layer on the European side of the ridge. The correlation is most intriguing for the fingers beneath the British Isles and the southern Scandinavian Mountains (sub-aerial, Fig. 8(b) and (c)). The low-velocity pattern along the Mid-Atlantic Ridge and particularly in the region of Iceland and the Kolbeinsey Ridge also resembles the pattern of estimated present day support fairly well (sub-aqueous, Fig. 8(a) and (c)).

Our S-velocity model gives strong support to the inferences of Jones et al. (2002) of wide-spread dynamic support in the North-Atlantic region by the Iceland plume. A sub-lithospheric flow of hotspot material in directions perpendicular to the Mid-Atlantic ridge is also argued for by the tomographic study of Delorey et al. (2007).

4.4. A lower-mantle source for the Iceland and Jan Mayen hotspots

Our model shows separate low-velocity conduits connecting the upper mantle hotspots of Iceland and Jan Mayen into the lower mantle. This is best seen in the vertical slices in Fig. 10(a) and (b), which cut approximately perpendicular to the Mid-Atlantic Ridge through the Iceland and Jan Mayen hotspots. Below both hotspots, low velocities extend through the transition zone into the lower mantle. Between the two hotspots (Fig. 10(c)), high velocities are imaged in the transition zone, indicating a separation of the conduits. The strength of the velocity perturbations in the conduits below a depth of 400 km varies between -0.5% and -2% with respect to the 1-D reference model. The conduits have a diameter of 300 to 400 km in the lower mantle and 100–200 km in the upper mantle. At depths above ~ 300 km, the conduits expand laterally to form the broad low-velocity region below the North Atlantic lithosphere.

The mantle surrounding the low-velocity conduits shows strong positive velocity perturbations. These are more pronounced at those depths where the conduits are weaker, particularly around the 660 and 410 km discontinuities. The 1-D reference model appears to systematically underestimate the velocity at these depths, possibly because it is not accurate when used as reference for full-waveform models. Independent from the reference model, a strong velocity contrast between the low-velocity conduits and the surrounding mantle is imaged at all depths.

The conduits beneath both the Iceland and Jan Mayen hotspots are tilted to the South-East, possibly reflecting the westward motion of the Mid-Atlantic Ridge with respect to a fixed hotspot reference frame (Morgan, 1983). The location where the Iceland conduit is imaged to cross the mantle transition zone agrees with results of Shen et al. (2002). They constrain the variation in transition zone thickness below Iceland using receiver functions and find the centre of a thinned region, indicative of a hot transition zone, to be located just south of Iceland. Their location corresponds precisely to the location of the Iceland conduit at a depth of 600 km in our model (Fig. 9). The results of Pritchard et al. (2000), who analyse patterns in waveform data recorded in Scotland and Norway, are also consistent with a South-East tilted low-velocity conduit.

The vertical cross-section in Fig. 10(b) suggests that the Jan Mayen conduit splits into two branches. Besides the main conduit leading in the direction of Jan Mayen, a second branch ends in the thickened

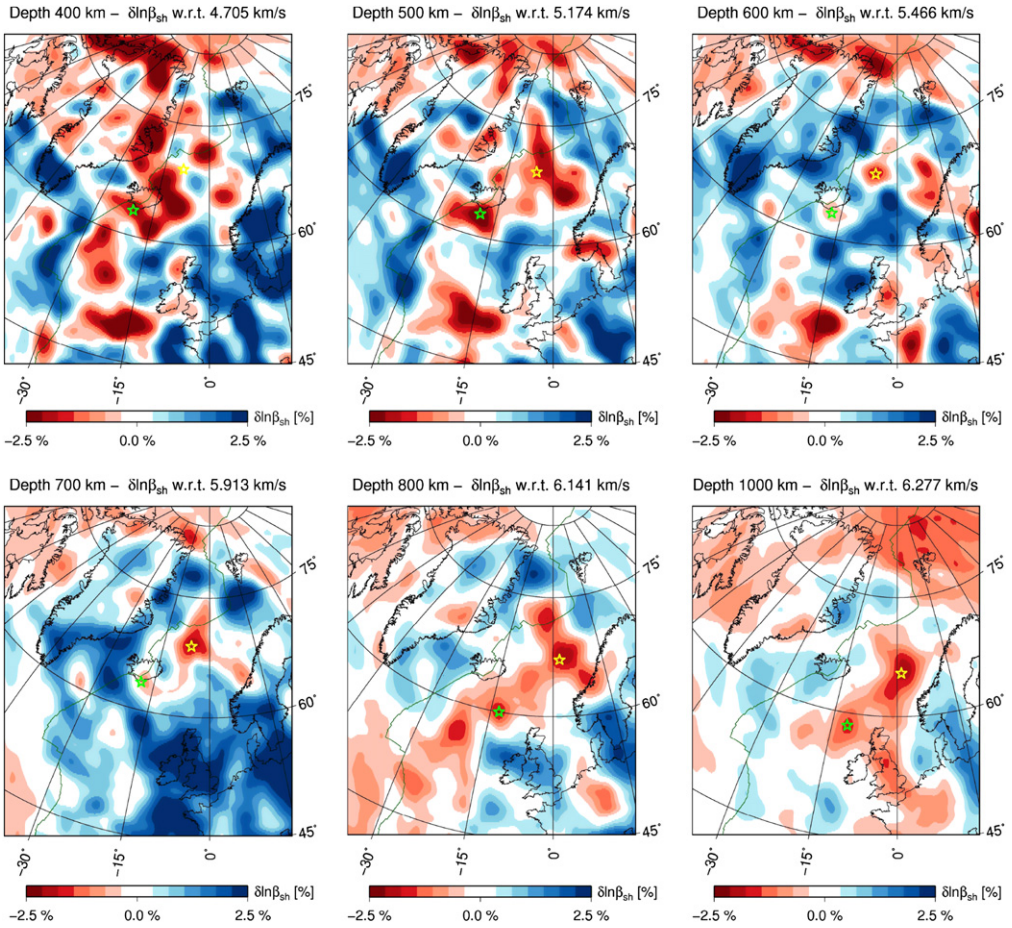

Fig. 9. Horizontal slices through the β_{sh}-component of model NA-IP, at depths between 400 and 1000 km. Perturbations are with respect to the reference velocity indicated in each panel. The stars indicate the location of the Iceland (green) and Jan Mayen (yellow) plume conduits, corresponding to the stars in the vertical slices of Fig. 10. (For interpretation of the references to colour in this figure caption, the reader is referred to the web version of this article.)

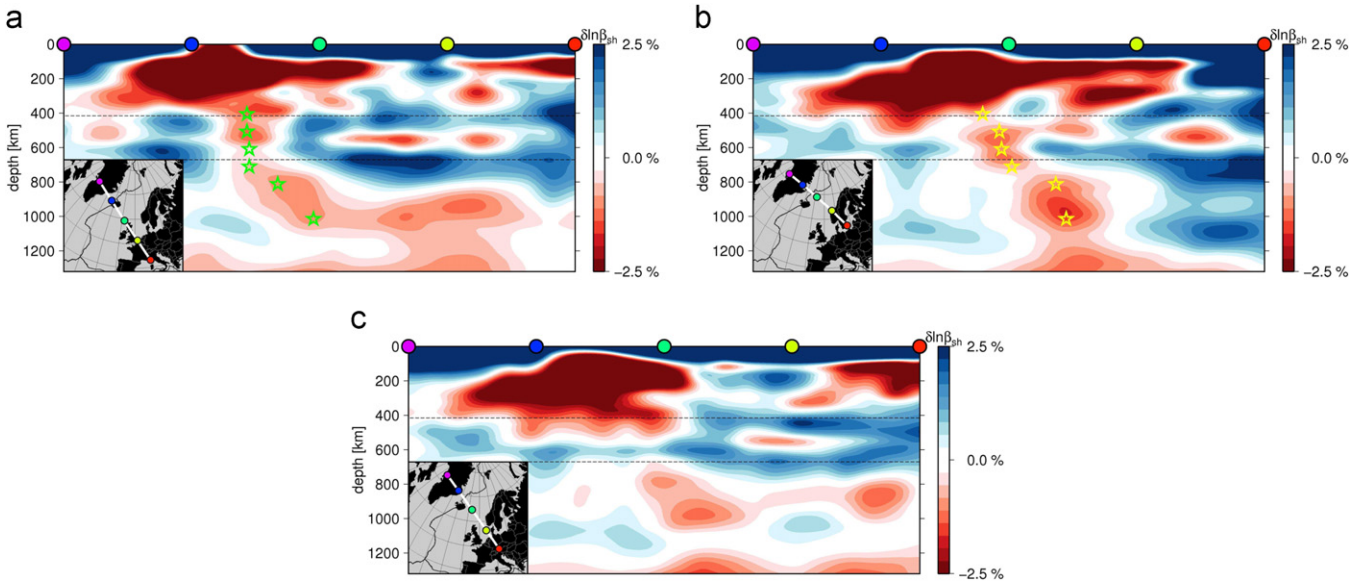

Fig. 10. Vertical slices through the β_{sh}-component of model NA-IP. The slices are roughly perpendicular to the Mid-Atlantic Ridge, the exact location is shown in the overview map in each panel. Perturbations are with respect to the 1-D reference model. The stars at different depths correspond to the stars in the horizontal slices in Fig. 9. (a) Slice through the Iceland plume conduit. (b) Slice through the Jan Mayen plume conduit. (c) Slice in-between the two plume conduits.

low-velocity zone beneath the lithosphere of the southern Scandinavian Mountains in Norway. The vertical cross-section suggests the branching to occur at a depth of about 500 km. However, an eastern branch closer to Norway is already visible at depths of 700 km and 800 km in Fig. 9. A branching plume could provide an explanation for the thickened low-velocity layer below the lithosphere of South-West Norway and the comparatively high elevation of the southern Scandinavian Mountains.

We constrained the temperature anomalies within the low-velocity conduits by converting the S-velocity model into a temperature model, based on mineral physics constraints (Stixrude and Lithgow-Bertelloni, 2005, 2011). With respect to the 1-D reference model, the excess temperature in both conduits exceeds 200 K throughout the lower mantle. In parts of the transition zone, in particular within the Iceland conduit, it decreases to about 50 K. With respect to the (faster and colder than average) mantle surrounding the conduits in the transition zone, however, the excess temperature still exceeds 120 K throughout the transition zone. In the upper mantle above the transition zone, the temperature anomaly again increases to values exceeding 200 K. Within the uppermost 300–400 km of the mantle, the excess temperature increases steeply and reaches 700 K below the hotspots and large parts of the oceanic lithosphere. Such high excess temperatures suggest that partial melting strongly contributes to the extremely low S-velocities in the uppermost mantle.

5. Conclusions

We have derived a high-resolution S-velocity model of the North Atlantic region, covering the upper and part of the lower mantle to a depth of 1300 km. The model is derived with non-linear full-waveform methods, the misfit between synthetic and observed waveforms is quantified with the instantaneous phase difference. S-waves and surface-waves together with their reflected and diffracted waves constrain the model, the data set consists of more than 4000 seismograms. Resolution tests using Point Spread Functions, an improved waveform fit and the correlation of the model with topographic, tectonic and gravimetric features confirm the geologic plausibility and high resolution of the model. The most important features of our model are:

(1) A well-resolved Mid-Atlantic Ridge and the presence of two separate hotspots beneath Iceland and beneath the northern part of the Kolbeinsey Ridge close to Jan Mayen. Separate hotspots are supported by geochemical (Schilling et al., 1999) and bathymetric evidence, but could not be identified in previous tomographic models. Velocities beneath both hotspots are reduced by up to −11%. A layer of low-velocity asthenosphere originating from the hotspots is imaged beneath much of the oceanic and part of the continental lithosphere of the North Atlantic region.

(2) A connection of the Iceland and Jan Mayen hotspots with post-rift uplift of South-West Scandinavia and parts of the British Isles is strongly supported by our model. Gravity-based estimates of present-day dynamic support in the North Atlantic region (Jones et al., 2002) agree very well with the imaged sub-lithospheric low-velocity pattern on the European side of the ridge. A correlation between a sub-lithospheric low-velocity layer and Neogene uplift is also found for eastern Greenland.
Our model is consistent with, and places into a larger context, previous smaller-scale studies of the Scandinavian region (Weidle and Maupin, 2008) and the British Isles (Arrowsmith et al., 2005; Davis et al., 2012). These studies suggest the presence of hotspot-related low velocities beneath uplifted regions.

(3) A lower-mantle source for both the Iceland and the Jan Mayen hotspots is suggested by our model. We image separate South-East-tilted low-velocity conduits beneath both hotspots, connecting through the transition zone into the lower mantle. Their diameter is 300–400 km in the lower mantle and 100–200 km in the upper mantle. Velocity perturbations within the conduits reach −0.5% to −2.0% with respect to the 1-D reference model, corresponding to excess temperatures of approximately 50–200 K. The 1-D reference model appears to underestimate velocities in the vicinity of the transition zone discontinuities, therefore the absolute velocity and temperature contrast between conduits and surrounding mantle is likely to be greater. The conduits are separated in the

transition zone and the upper mantle, but a possible full separation in the lower mantle cannot be clearly inferred from our model.

The location of the imaged Iceland conduit is consistent with the receiver function study of Shen et al. (2002), who observe a locally thinned transition zone south of Iceland. The Jan Mayen plume appears to branch at a depth of about 500 km, or possibly deeper. The second branch is directed towards south-western Norway, where a thickened low-velocity layer beneath the continental lithosphere is imaged.

(4) The model resolves the Greenland and Baltic Shields in great detail. We image a East–West oriented corridor of thinned lithosphere beneath Greenland, approximately correlating with the reconstructed track of the Iceland hotspot between 70 Ma and 35 Ma (Lawver and Müller, 1994). The hotspot may have weakened the lithosphere while it was located beneath Greenland. A sharp boundary between the thick, Precambrian lithosphere of the Baltic Shield and the thinner continental lithosphere of South-West Norway and the Danish Basin is imaged in our model. The sub-lithospheric low-velocity layer cannot cross this boundary and is confined to the shallower lithosphere of South-West Scandinavia.

Acknowledgements

This work was financed by the Netherlands Research Centre for Integrated Solid Earth Sciences under grants ISES-NorMar-2.6 and ISES-UU-PC-cluster. Use of the Huygens IBM p6 supercomputer at SARA Amsterdam was sponsored by the National Computing Facilities Foundation (N.C.F.) under the project SH-161-09 with financial support from the Netherlands Organisation for Scientific Research (N.W.O.). We are grateful to Theo van Zessen for maintaining the HPC clusters STIG and GRIT at the Department of Earth Sciences at Utrecht University. Nicky White and Stephen Jones kindly provided the long-wavelength gravity field data and gave inspiring comments. We thank Hans-Peter Bunge for helpful initial suggestions on the interpretation of the model, and Laura Cobden for providing the mineral physics constraints used for the temperature conversion. The constructive comments of Christophe Zaroli and Hejun Zhu greatly improved the manuscript. All figures were prepared with the Generic Mapping Tools (Wessel and Smith, 1998).

References

Allen, R., Nolet, G., Morgan, W., Vogfjord, K., Bergsson, B., Erlendsson, P., Foulger, G., Jakobsdottir, S., Julian, B., Pritchard, M., Ragnarsson, S., Stefansson, R., 2002. Imaging the mantle beneath Iceland using integrated seismological techniques. J. Geophys. Res. 107, 2325.

Arrowsmith, S., Kendall, M., White, N., VanDecar, J., Booth, D., 2005. Seismic imaging of a hot upwelling beneath the British Isles. Geology 33, 345–348.

Bijwaard, H., Spakman, W., 1999. Tomographic evidence for a narrow whole mantle plume below Iceland. Earth Planet. Sci. Lett. 166, 121–126.

Bjarnason, I., Silver, P., Rümpker, G., Solomon, S., 2002. Shear wave splitting across the Iceland hot spot: results from the ICEMELT experiment. J. Geophys. Res. 107, 2382.

Bott, M., Bott, J., 2004. The Cenozoic uplift and earthquake belt of mainland Britain as a response to an underlying hot, low-density upper mantle. J. Geol. Soc. 161, 19–29.

Bozdağ, E., Trampert, J., Tromp, J., 2011. Misfit functions for full waveform inversion based on instantaneous phase and envelope measurements. Geophys. J. Int. 185, 845–870.

Carminati, E., Cuffaro, M., Doglioni, C., 2009. Cenozoic uplift of Europe. Tectonics 28, TC4016.

Davis, M.W., White, N.J., Priestley, K.F., Baptie, B.J., Tilmann, F.J., 2012. Crustal structure of the British Isles and its epeirogenic consequences. Geophys. J. Int. 190, 705–725.

Delorey, A., Dunn, R., Gaherty, J., 2007. Surface wave tomography of the upper mantle beneath the Reykjanes Ridge with implications for ridge–hot spot interaction. J. Geophys. Res. 112, B08313.

Doré, A.G., Cartwright, J.A., Stoker, M.S., Turner, J.P., White, N.J., 2002. Exhumation of the North Atlantic margin: introduction and background. Geol. Soc. London Spec. Publ. 196, 1–12.

Du, Z., Vinnik, L., Foulger, G., 2006. Evidence from P-to-S mantle converted waves for a flat '660-km' discontinuity beneath Iceland. Earth Planet. Sci. Lett. 241, 271–280.

Duncan, W., Green, P., Duddy, I., 1998. Source rock burial history and seal effectiveness: key facets to understanding hydrocarbon exploration potential in the East and Central Irish Sea Basins. AAPG Bull. 82, 1401–1415.

Dziewonski, A.M., Anderson, D.L., 1981. Preliminary reference earth model. Phys. Earth Planet. In. 25, 297–356.

Ebbing, J., England, R., Korja, T., Lauritsen, T., Olesen, O., Stratford, W., Weidle, C., 2012. Structure of the Scandes lithosphere from surface to depth. Tectonophysics 536, 1–24.

Ebbing, J., Olesen, O., 2005. The Northern and Southern Scandes-structural differences revealed by an analysis of gravity anomalies, the geoid and regional isostasy. Tectonophysics 411, 73–87.

Fichtner, A., Bunge, H., Igel, H., 2006. The adjoint method in seismology: I. Theory. Phys. Earth Planet. In. 157, 86–104.

Fichtner, A., Igel, H., 2008. Efficient numerical surface wave propagation through the optimization of discrete crustal models—a technique based on non-linear dispersion curve matching. Geophys. J. Int. 173, 519–533.

Fichtner, A., Kennett, B.L.N., Igel, H., Bunge, H.P., 2009. Full seismic waveform tomography for upper-mantle structure in the Australasian region using adjoint methods. Geophys. J. Int. 179, 1703–1725.

Fichtner, A., Trampert, J., 2011. Resolution analysis in full waveform inversion. Geophys. J. Int. 187, 1604–1624.

Fletcher, R., Reeves, C., 1964. Function minimization by conjugate gradients. Comput. J. 7, 149–154.

Foulger, G., Anderson, D., 2005. A cool model for the Iceland hotspot. J. Volcanol. Geotherm. Res. 141, 1–22.

Foulger, G., Pritchard, M., Julian, B., Evans, J., Allen, R., Nolet, G., Morgan, W., Bergsson, B., Erlendsson, P., Jakobsdottir, S., et al., 2001. Seismic tomography shows that upwelling beneath Iceland is confined to the upper mantle. Geophys. J. Int. 146, 504–530.

Foulger, G.R., 2012. Are 'hot spots' hot spots? J. Geodyn. 58, 1–28.

George, T., 1966. Geomorphic evolution in Hebridean Scotland. Scott. J. Geol. 2, 1–34.

Grand, S., 2002. Mantle shear–wave tomography and the fate of subducted slabs. Philos. Trans. R. Soc. Lond. A 360, 2475–2491.

Green, P., 1989. Thermal and tectonic history of the East Midlands shelf (onshore UK) and surrounding regions assessed by apatite fission track analysis. J. Geol. Soc. 146, 755–773.

Hall, A., Bishop, P., 2002. Scotland's denudational history: an integrated view of erosion and sedimentation at an uplifted passive margin. Geol. Soc. London Spec. Publ. 196, 271–290.

Holford, S., Green, P., Turner, J., Williams, G., Hillis, R., Tappin, D., Duddy, I., 2008. Evidence for kilometre-scale Neogene exhumation driven by compressional deformation in the Irish Sea Basin system. Geol. Soc. London Spec. Publ. 306, 91–119.

Hwang, Y.K., Ritsema, J., van Keken, P.E., Goes, S., Styles, E., 2011. Wavefront healing renders deep plumes seismically invisible. Geophys. J. Int. 187, 273–277.

Japsen, P., 1997. Regional Neogene exhumation of Britain and the western North Sea. J. Geol. Soc. 154, 239–247.

Japsen, P., Bidstrup, T., Lidmar-Bergström, K., 2002. Neogene uplift and erosion of southern Scandinavia induced by the rise of the South Swedish Dome. Geol. Soc. London Spec. Publ. 196, 183–207.

Japsen, P., Chalmers, J., 2000. Neogene uplift and tectonics around the North Atlantic: overview. Global Planet. Change 24, 165–173.

Japsen, P., Green, P., Nielsen, L., Rasmussen, E., Bidstrup, T., 2007. Mesozoic–Cenozoic exhumation events in the eastern North Sea Basin: a multidisciplinary study based on palaeothermal, palaeoburial, stratigraphic and seismic data. Basin Res. 19, 451–490.

Johnson, C., Gallagher, K., 2000. A preliminary Mesozoic and Cenozoic denudation history of the North East Greenland onshore margin. Global Planet. Change 24, 261–274.

Jones, S., White, N., Clarke, B., Rowley, E., Gallagher, K., 2002. Present and past influence of the Iceland Plume on sedimentation. Geol. Soc. London Spec. Publ. 196, 13–25.

Keller, W., Anderson, D., Clayton, R., 2000. Resolution of tomographic models of the mantle beneath Iceland. Geophys. Res. Lett. 27, 3993–3996.

Lawver, L., Müller, R., 1994. Iceland hotspot track. Geology 22, 311–314.

Legendre, C., Meier, T., Lebedev, S., Friederich, W., Viereck-Götte, L., 2012. A shear wave velocity model of the European upper mantle from automated inversion of seismic shear and surface waveforms. Geophys. J. Int. 191, 282–304.

Mathiesen, A., Bidstrup, T., Christiansen, F., 2000. Denudation and uplift history of the Jameson Land Basin, East Greenland-constrained from maturity and apatite fission track data. Global Planet. Change 24, 275–301.

Morgan, J., 1983. Hotspot tracks and the early rifting of the Atlantic. Tectonophysics 94, 123–139.

Morgan, W.J., 1971. Convection plumes in the lower mantle. Nature 230, 42–43.

Pascal, C., Olesen, O., 2009. Are the Norwegian mountains compensated by a mantle thermal anomaly at depth? Tectonophysics 475, 160–168.

Pilidou, S., Priestley, K., Debayle, E., Gudmundsson, O., 2005. Rayleigh wave tomography in the North Atlantic: high resolution images of the Iceland, Azores and Eifel mantle plumes. Lithos 79, 453–474.
Pritchard, M.J., Foulger, G.R., Julian, B.R., Fyen, J., 2000. Constraints on a plume in the mid-mantle beneath the Iceland region from seismic array data. Geophys. J. Int. 143, 119–128.
Redfield, T., Osmundsen, P., Hendriks, B., 2005. The role of fault reactivation and growth in the uplift of western Fennoscandia. J. Geol. Soc. 162, 1013–1030.
Rickers, F., Fichtner, A., Trampert, J., 2012. Imaging mantle plumes with instantaneous phase measurements of diffracted waves. Geophys. J. Int. 190, 650–664.
Ritsema, J., Allen, R.M., 2003. The elusive mantle plume. Earth Planet. Sci. Lett. 207, 1–12.
Ritsema, J., Deuss, A., Van Heijst, H., Woodhouse, J., 2011. S40RTS: a degree-40 shear-velocity model for the mantle from new Rayleigh wave dispersion, teleseismic traveltime and normal-mode splitting function measurements. Geophys. J. Int. 184, 1223–1236.
Ritsema, J., van Heijst, H., Woodhouse, J., 1999. Complex shear wave velocity structure imaged beneath Africa and Iceland. Science 286, 1925–1928.
Rohrman, M., van der Beek, P., 1996. Cenozoic postrift domal uplift of North Atlantic margins: an asthenospheric diapirism model. Geology 24, 901–904.
Rohrman, M., van der Beek, P., Andriessen, P., Cloetingh, S., 1995. Meso-Cenozoic morphotectonic evolution of southern Norway: Neogene domal uplift inferred from apatite fission track thermochronology. Tectonics 14, 704–718.
Schilling, J., 1985. Upper mantle heterogeneities and dynamics. Nature 314, 62–67.
Schilling, J., Kingsley, R., Fontignie, D., Poreda, R., Xue, S., 1999. Dispersion of the Jan Mayen and Iceland mantle plumes in the Arctic: a He–Pb–Nd–Sr isotope tracer study of basalts from the Kolbeinsey, Mohns, and Knipovich Ridges. J. Geophys. Res. 104 10543-10.
Shen, Y., Solomon, S., Bjarnason, I., Nolet, G., Morgan, W., Allen, R., Vogfjörd, K., Jakobsdóttir, S., Stefánsson, R., Julian, B., et al., 2002. Seismic evidence for a tilted mantle plume and north–south mantle flow beneath Iceland. Earth Planet. Sci. Lett. 197, 261–272.
Shen, Y., Solomon, S.C., Bjarnason, I.T., Wolfe, C.J., 1998. Seismic evidence for a lower-mantle origin of the Iceland plume. Nature 395, 62–65.
Stixrude, L., Lithgow-Bertelloni, C., 2005. Thermodynamics of mantle minerals—I. Physical properties. Geophys. J. Int. 162, 610–632.
Stixrude, L., Lithgow-Bertelloni, C., 2011. Thermodynamics of mantle minerals—II. Phase equilibria. Geophys. J. Int. 184, 1180–1213.
Tape, C., Liu, Q., Maggi, A., Tromp, J., 2010. Seismic tomography of the southern California crust based on spectral-element and adjoint methods. Geophys. J. Int. 180, 433–462.
Tapley, B., Ries, J., Bettadpur, S., Chambers, D., Cheng, M., Condi, F., Poole, S., 2007. The GGM03 mean earth gravity model from GRACE. In: AGU Fall Meeting Abstracts, p. 03.
Tarantola, A., 1984. Inversion of seismic reflection data in the acoustic approximation. Geophysics 49, 1259–1266.
Tromp, J., Tape, C., Liu, Q., 2005. Seismic tomography, adjoint methods, time reversal and banana-doughnut kernels. Geophys. J. Int. 160, 195–216.
Tryggvason, K., Husebye, E., Stefánsson, R., 1983. Seismic image of the hypothesized Icelandic hot spot. Tectonophysics 100, 97–118.
Vågnes, E., Amundsen, H., 1993. Late Cenozoic uplift and volcanism on Spitsbergen: caused by mantle convection? Geology 21, 251–254.
Weidle, C., Maupin, V., 2008. An upper-mantle S-wave velocity model for Northern Europe from Love and Rayleigh group velocities. Geophys. J. Int. 175, 1154–1168.
Wessel, P., Smith, W., 1998. New, improved version of generic mapping tools released. EOS Trans. Am. Geophys. Un. 79, 579.
White, R., McKenzie, D., 1989. Magmatism at rift zones: the generation of volcanic continental margins and flood basalts. J. Geophys. Res. 94, 7685–7729.
Wolfe, C.J., Th.Bjarnason, I., VanDecar, J.C., Solomon, S.C., 1997. Seismic structure of the Iceland mantle plume. Nature 385, 245–247.
Zhao, D., 2004. Global tomographic images of mantle plumes and subducting slabs: insight into deep earth dynamics. Phys. Earth Planet. In. 146, 3–34.
Zhu, H., Bozdag, E., Peter, D., Tromp, J., 2012. Structure of the European upper mantle revealed by adjoint tomography. Nat. Geosci. 5, 493–498.